Geophysical Journal International

Geophys. J. Int. (2017) **210,** 223–227
Advance Access publication 2017 April 26
GJI Marine geosciences and applied geophysics

doi: 10.1093/gji/ggx159

EXPRESS LETTER

Fracture connectivity can reduce the velocity anisotropy of seismic waves

J. Germán Rubino,[1] Eva Caspari,[2] Tobias M. Müller[3] and Klaus Holliger[2]

[1] *CONICET, Centro Atómico Bariloche - CNEA, San Carlos de Bariloche, Argentina. E-mail: german.rubino@cab.cnea.gov.ar*
[2] *Applied and Environmental Geophysics Group, Institute of Earth Sciences, University of Lausanne, Lausanne, Switzerland*
[3] *Commonwealth Scientific and Industrial Research Organization, Energy, Perth, Australia*

Accepted 2017 April 24. Received 2017 April 19; in original form 2016 December 26

SUMMARY

The degree of connectivity of fracture networks is a key parameter that controls the hydraulic properties of fractured rock formations. The current understanding is that this parameter does not alter the effective elastic properties of the probed medium and, hence, cannot be inferred from seismic data. However, this reasoning is based on static elasticity, which neglects dynamic effects related to wave-induced fluid pressure diffusion (FPD). Using a numerical upscaling procedure based on the theory of quasi-static poroelasticity, we provide the first evidence to suggest that fracture connectivity can reduce significantly velocity anisotropy in the seismic frequency band. Analyses of fluid pressure fields in response to the propagation of seismic waves demonstrate that this reduction of velocity anisotropy is not due to changes of the geometrical characteristics of the probed fracture networks, but rather related to variations of the stiffening effect of the fracture fluid in response to FPD. These results suggest that accounting for FPD effects may not only allow for improving estimations of geometrical and mechanical properties of fracture networks, but may also provide information with regard to the effective hydraulic properties.

Key words: Fracture and flow; Numerical modelling; Seismic anisotropy.

1 INTRODUCTION

Fractures are very common in the shallower parts of the Earth's crust and they tend to dominate the mechanical and hydraulic properties of the embedding rocks. Therefore, the detection and characterization of fracture networks are important objectives in a wide variety of disciplines, including hydrocarbon exploration, hydrogeology, nuclear waste storage, CO_2 sequestration, and tunnel engineering (e.g. Liu *et al.* 2000; Maultzsch *et al.* 2003).

It is widely accepted that seismic velocity anisotropy is an important parameter for assessing fracture orientation and fracture density (e.g. Tsvankin *et al.* 2010; Liu & Martinez 2012). Estimates of fracture length and spacing, on the other hand, require additional analyses of the frequency dependency of anisotropy and seismic amplitudes (e.g. Maultzsch *et al.* 2003; Liu & Martinez 2012). Currently, the determination of fracture parameters controlling the effective hydraulic properties remains largely unsuccessful without additional information, such as that provided by production data (e.g. Will *et al.* 2004). One reason for this lack of success may be that seismic anisotropy analyses are typically based on effective medium approaches, treating fractured formations as elastic composites. These frameworks ignore the possibility that seismic waves induce fluid pressure gradients and that the subsequent fluid pressure diffusion (FPD) can affect the overall elastic properties. These physical oversimplifications can have important consequences for seismic fracture network characterization. Indeed, working within the scope of linear elasticity, Grechka & Kachanov (2006) found that the degree of fracture network connectivity has a rather negligible effect on the effective seismic response. Conversely, using a poroelastic approach, Rubino *et al.* (2013, 2014) recently demonstrated that in the presence of connected fractures there is an attenuation peak and velocity dispersion related to FPD within the connected fractures as well as a significant reduction of the attenuation and dispersion due to FPD between the fractures and the embedding background. The results indicate that fracture connectivity does indeed have a substantial effect on the effective seismic response, but the corresponding impact on velocity anisotropy remains unexplored. Given that fracture connectivity is a key parameter controlling the effective hydraulic properties and that seismic anisotropy is a robust seismic attribute, potential effects of fracture connectivity on velocity anisotropy may have important implications for the characterization of fracture networks.

In this work, we use a numerical upscaling procedure (Rubino *et al.* 2016) based on the theory of quasi-static poroelasticity (Biot 1941) to determine the effective anisotropic seismic properties of 2-D models of fractured rocks. We compare the results for synthetic

samples containing two orthogonal fracture sets with varying degrees of connectivity, which allows us to determine the influence of this parameter on seismic velocity anisotropy.

2 NUMERICAL UPSCALING

To determine the anisotropic seismic properties of fractured rocks taking into account FPD effects, we employ a numerical upscaling procedure recently presented by Rubino *et al.* (2016). We consider a square sample that is representative of the fractured formation of interest. It contains fractures in the mesoscopic scale range, that is, smaller than the prevailing wavelengths but larger than the typical pore size. We model the seismic response in a poroelastic framework (Biot 1941) with the fractures represented as highly compliant features of very high porosity and permeability (Rubino *et al.* 2013). In order to estimate the effective seismic properties, we apply three relaxation tests. We first apply homogeneous time-harmonic normal displacements on the top and bottom boundaries of the sample, while the lateral boundaries are confined. The fluid is not allowed to flow into the sample or out of it. The second test is similar to the previous one, but the normal displacements are applied on the lateral boundaries of the sample. Finally, in the third test, we apply oscillatory simple shear displacements to the sample.

The resulting solid and relative fluid displacement fields are obtained by solving the quasi-static isotropic poroelastic equations (Biot 1941). Under the assumption that the volume average response of the probed rock can be represented by that of an equivalent homogeneous anisotropic viscoelastic solid, the volume averages of the stress and strain components resulting from each test are related through an equivalent Voigt stiffness matrix. The components of this matrix are computed, for each frequency, following a least-squares procedure. The phase velocity of *P*- and *S*-waves as functions of incidence angle and frequency are computed following a standard procedure for anisotropic viscoelastic solids. Please note that, due to the 2-D nature of the numerical upscaling procedure, the *S*-wave corresponds to that polarized within the considered plane.

3 SYNTHETIC ROCK SAMPLES

We consider 2-D numerical samples with a side length of 72 cm containing 150 vertical and 150 horizontal fractures (Fig. 1). The fractures have a rectangular geometry with an aperture and a length of 0.06 cm and 4.2 cm, respectively. Based on the definition of Kachanov (1992), this corresponds to a fracture density of 0.2552. The scaling parameter (fracture length/domain length) is sufficiently small so that finite-size effects are negligible (Saenger & Shapiro 2002), while the domain is sufficiently large to be statistically and physically representative (Caspari *et al.* 2016). This assures that our experiments are suitable to infer the effective seismic properties of the considered fractured media.

We analyse three different scenarios for uniformly distributed and, thus, uncorrelated fracture centres: unconnected fractures (Fig. 1a), partially connected fractures (Fig. 1b), and almost all fractures having at least one connection but no percolating clusters being formed (Fig. 1c). In the first scenario, we successively place fracture centres into the model updating in each step the available positions so that the fractures are not connected, while in the last scenario, we force each vertical fracture to have at least one connection. Since, in a strict sense, this violates the condition of uncorrelated fracture centres, we check, for each realization, the deviation from a uniform random distribution. We then choose the realizations with the most homogeneous distributions of fracture centres to minimize geometrical differences between the three scenarios. For the scenario of partially connected fractures, we do not control the number of fracture connections.

The water saturating the pore volume has a bulk modulus $K_w = 2.25$ GPa, a density $\rho_w = 1090$ Kg m^{-3}, and a shear viscosity $\eta_w = 0.001$ Pa s. The properties of the background material are assumed to correspond to a homogeneous and isotropic tight sandstone. For the solid grains, we consider a bulk modulus $K_s^b = 37$ GPa, a shear modulus $\mu_s^b = 44$ GPa, and a density $\rho_s^b = 2650$ Kg m^{-3}. For the dry frame, we use a porosity $\phi^b = 0.05$, a permeability $\kappa^b = 10^{-5}$ mD $\simeq 10^{-20}$ m^2, a drained-frame bulk modulus $K_m^b = 31.5$ GPa and a drained-frame shear modulus $\mu_m^b = 37.4$ GPa.

For the fractures, we assume that at the grain level the physical properties are the same as those of the background. For the dry-frame properties, we use $K_m^f = 0.04$ GPa and $\mu_m^f = 0.02$ GPa (Rubino *et al.* 2014), while we set the porosity to $\phi^f = 0.8$ and the permeability to $\kappa^f = 1000$ D $\simeq 10^{-9}$ m^2.

4 RESULTS

4.1 Sensitivity of velocity anisotropy to the degree of fracture connectivity

Fig. 2(a) shows the *P*-wave phase velocity of the samples depicted in Fig. 1 as a function of the incidence angle measured with respect

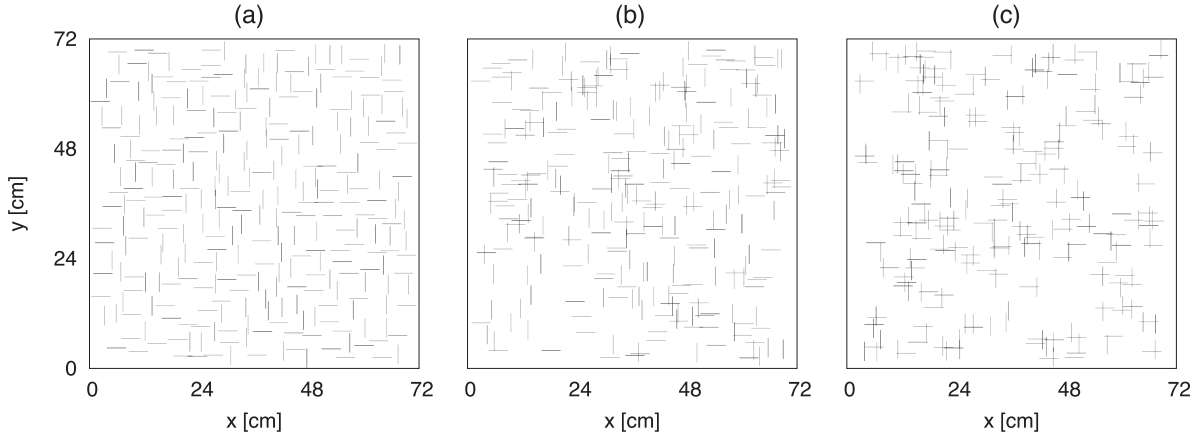

Figure 1. Synthetic rock samples having the same fracture density, but different degrees of fracture connectivity. In sample (a) all fractures are unconnected, in sample (b) the average number of connections per fracture is ∼0.7, while in sample (c) it is ∼1.5.

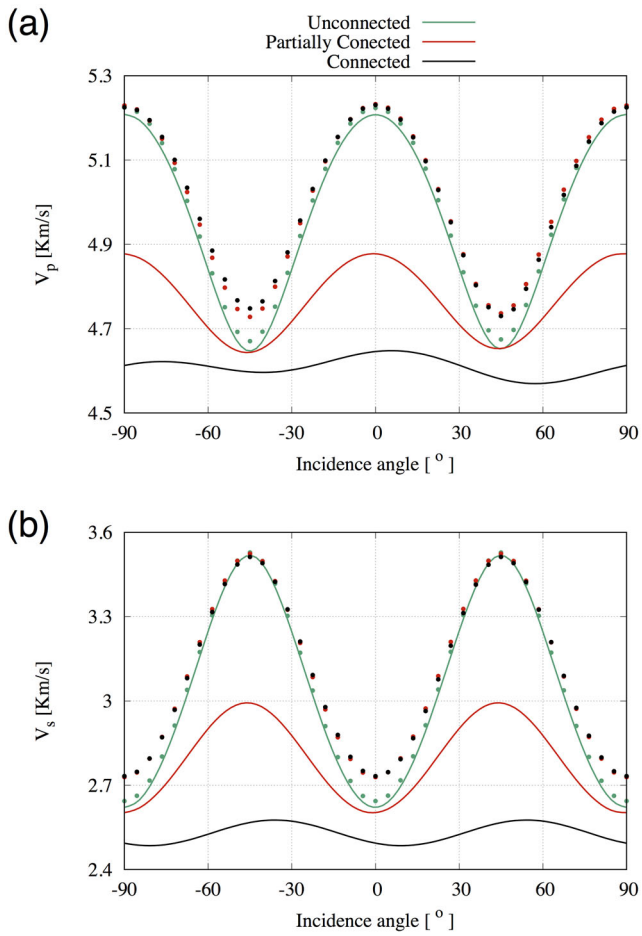

Figure 2. (a) *P*- and (b) *S*-wave velocities as functions of incidence angle for the samples shown in Fig. 1. Solid lines correspond to a frequency of 100 Hz, whereas dots denote the corresponding high-frequency, or elastic, limits.

to the vertical and for a frequency of 100 Hz (solid lines). We observe that, in the unconnected case (sample (a) in Fig. 1), the level of anisotropy is very high (solid green line), with maximum velocities of ∼5.2 km s^{-1} prevailing for vertical and horizontal wave propagation and minimum values of ∼4.65 km s^{-1} at incidence angles $\theta = \pm 45^{\circ}$. As the level of fracture connectivity increases, the level of anisotropy is significantly reduced. Indeed, in the connected case (sample (c) in Fig. 1), velocity anisotropy is almost inexistent (solid black line). For the sample having a partially connected fracture network (Fig. 1b), the level of anisotropy lies between those of the unconnected and connected cases (solid red line). Note that the discrepancies in terms of velocity anisotropy are mainly due to velocity differences for horizontal and vertical wave propagation. For $\theta \simeq \pm 45^{\circ}$, the velocities for the three samples are rather similar.

Fig. 2(b) shows the results for the *S*-wave velocity. In the unconnected scenario (solid green line), there is strong anisotropy, with maximum velocities of ∼3.5 km s^{-1} for $\theta \simeq \pm 45^{\circ}$ and minimum velocities of ∼2.6 km s^{-1} for vertical or horizontal wave propagation. A dramatic reduction of the level of anisotropy occurs as the degree of fracture connectivity increases, with anisotropy virtually inexistent in the connected case (solid black line). The sample with a partially connected fracture network exhibits an intermediate behaviour (solid red line). We observe that, in the case of *S*-waves, the change of anisotropy with the degree of fracture connectivity is mainly due to velocity discrepancies arising for $\theta \simeq \pm 45^{\circ}$. For horizontal or vertical wave propagation, the *S*-wave velocity is not particularly sensitive to the degree of fracture connectivity.

Fig. 2 also shows the responses in the high-frequency limit (dots), which were obtained by using the numerical upscaling procedure for a frequency much higher than the transition frequencies of the two manifestations of wave-induced FPD arising in the presence of connected fractures (Rubino *et al.* 2013, 2014). This end-member scenario describes the unrelaxed state, wherein there is not enough time in a half wave cycle for relative fluid–solid motion to occur and, thus, resembles wave propagation in an equivalent elastic composite. In this situation, both *P*- and *S*-wave velocities and their anisotropies are practically independent of fracture connectivity (Fig. 2), which conforms with the results of Grechka & Kachanov (2006). An important conclusion of this analysis is therefore that the anisotropy reduction with increasing fracture connectivity at 100 Hz is a true dynamic effect due to FPD and not related to variations of the geometrical aspects of the probed fracture networks.

4.2 Physical interpretation

The main result of our simulations is the reduction of velocity anisotropy with increasing degree of fracture connectivity. In order to explore the physical origins of this phenomenon, it is important to understand that in the presence of connected fractures two manifestations of FPD prevail (Rubino *et al.* 2013, 2014). One is due to fluid pressure exchange between the fractures and the background. The characteristic frequency of the associated maximum attenuation and velocity dispersion is directly proportional to the background permeability. For low-permeability formations, this velocity dispersion prevails at very low frequencies, typically well below the seismic range. For the examples considered here, this effect occurs for frequencies around 10^{-4} Hz. The second manifestation of FPD is due to fluid pressure exchanges within connected fractures. The frequency range where this mechanism leads to velocity dispersion is directly proportional to the fracture permeability and inversely proportional to the length of the fractures. Due to the typically very high permeabilities of fractures, this manifestation of FPD tends to prevail at frequencies well above the seismic range for cm- to m-scale fractures. In this work, it arises for frequencies around 10^{6} Hz. Therefore, there exists a wide, constant-velocity plateau between the two frequency ranges where velocity dispersion occurs which, in the case of low-permeability formations, tends to cover the seismic frequency band. For frequencies within this band, there is not enough time in a half wave cycle for communication between fractures and background and, thus, fractures behave as hydraulically sealed. Conversely, in the presence of connected fractures, there is enough time for the fluid pressure within the fractures to equilibrate. Therefore, the stiffening effect of the fluid saturating the fractures diminishes and hence alters the seismic velocity. This effect, which depends on the incidence angle, can thus affect the seismic velocity anisotropy.

To explore the physical causes in more detail, we include in Fig. 3 a blowup of the real part of the fluid pressure in response to an incident *P*-wave obtained following the procedure by Rubino *et al.* (2016). In the case of vertical wave propagation for the unconnected scenario (Fig. 3a), the wave-induced compression increases significantly the fluid pressure inside the horizontal fractures. This pressure opposes the compression applied by the wave and thus reduces the deformability of the fractures, thereby producing a stiffening effect. Moreover, due to the low background permeability, FPD between this region and the fractures is negligible. The lack of FPD

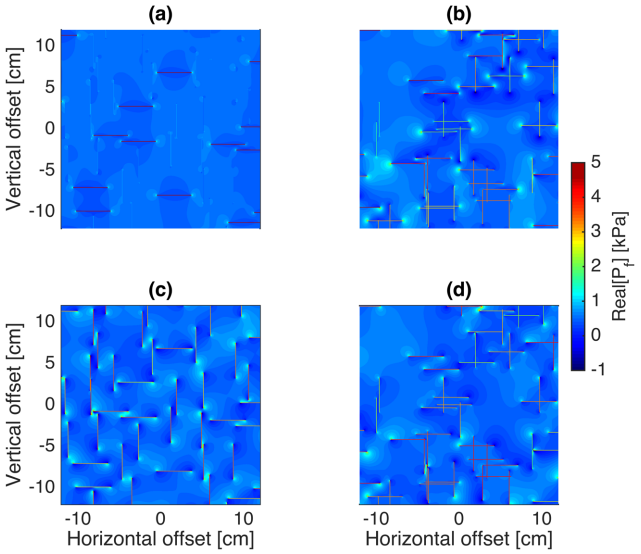

Figure 3. Blowup of the real part of the fluid pressure in response to the propagation of a *P*-wave travelling through the central parts of the samples with (a, c) unconnected and (b, d) connected fractures (Fig. 1). The incidence angles are (a, b) $\theta = 0$ and (c, d) $\theta = 45^\circ$, and the frequency is 100 Hz. The axes indicate the corresponding offsets from the centre of the sample.

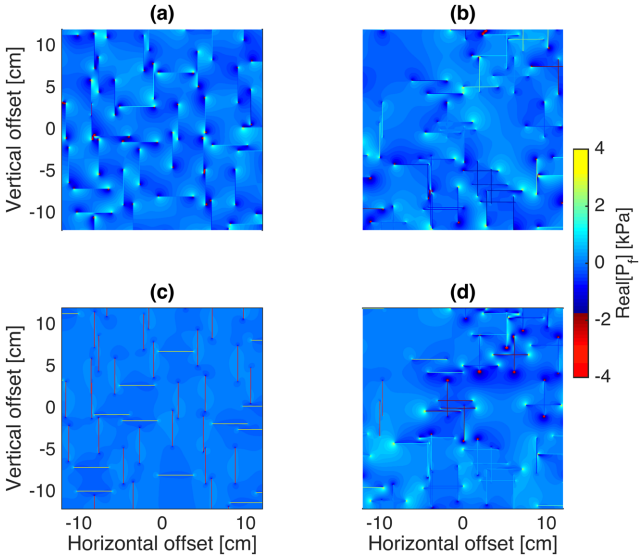

Figure 4. Blowup of the real part of the fluid pressure in response to the propagation of an *S*-wave travelling through the central parts of the samples with (a, c) unconnected and (b, d) connected fractures (Fig. 1). The incidence angles are (a, b) $\theta = 0$ and (c, d) $\theta = 45^\circ$, and the frequency is 100 Hz.

explains the good agreement between the velocities in the seismic frequency band and in the high-frequency limit (Fig. 2a). In the connected scenario, the fluid of the horizontal fractures has enough time during a half cycle to release its pressure into the connected vertical fractures. This fluid pressure exchange can be clearly seen in Fig. 3(b) as a reduction of the fluid pressure in the horizontal fractures compared with the unconnected scenario and an increase of the fluid pressure inside the connected vertical fractures. The fluid pressure relaxation implies that the stiffening effect of the fluid inside the horizontal fractures is reduced and the sample behaves as if it was softer, thus resulting in a lower *P*-wave velocity compared to the high-frequency limit. This behaviour explains the reduction of *P*-wave velocity for incidence angles close to 0° and 90° as fracture connectivity increases (Fig. 2a).

For $\theta = 45^\circ$ in the unconnected scenario, both fracture sets are compressed by the *P*-wave and all fractures experience a similar fluid pressure increase (Fig. 3c). The lack of significant fluid pressure differences between horizontal and vertical fractures implies that when the fractures become connected, there is no significant fluid pressure exchange, as can be verified in Fig. 3(d), where we observe that the fluid pressure values inside the connected fractures are comparable to those corresponding to the unconnected case (Fig. 3c). The lack of fluid pressure release implies that the stiffening effect of the fluid saturating the fractures does not change when fractures become connected. Correspondingly, for $\theta \simeq \pm 45^\circ$ the discrepancies between *P*-wave velocities for connected and unconnected scenarios are largely negligible and the velocities turn out to be comparable to their high-frequency limits (Fig. 2a).

The impact of FPD on the stiffening effect of the fracture fluid therefore strongly depends on the incidence angle. In the connected scenario, this is responsible for the reduction of the contrast between *P*-wave velocities for horizontal or vertical wave propagation with respect to those for $\theta = \pm 45^\circ$ and, thus, for the reduction in *P*-wave anisotropy.

Fig. 4 shows a blowup of the real part of the fluid pressure in response to an incident *S*-wave. In the unconnected case and for vertical wave propagation, the induced fluid pressure inside the fractures is negligible (Fig. 4a). Consequently, when the fractures become connected, the fluid pressure does not change significantly (Fig. 4b) and the impact on the *S*-wave velocity is rather small (Fig. 2b). Due to the lack of FPD, there is also good agreement with the corresponding high-frequency limit for both cases.

For $\theta = 45^\circ$ the *S*-wave induces high absolute values of fluid pressure inside both fractures sets in the unconnected scenario (Fig. 4c). However, while there is an increase of pressure in the horizontal fractures, the pressure decreases in the vertical ones. These fluid pressure changes tend to counteract the deformation and, thus, increase the overall rigidity. Since FPD across the fractures is not possible, the resulting velocity is comparable to that of the high-frequency limit (Fig. 2b). For the connected scenario, a particular effect occurs. Since the induced pressures are positive and negative in the horizontal and vertical fractures, respectively, the resulting pressure gradient gets very large when the fractures become connected. FPD then reduces the magnitude of the fluid pressure in both fracture sets and, thus, its effect on the overall rigidity of the rock. As a result, the *S*-wave velocity significantly diminishes with respect to the high-frequency limit (Fig. 2b). This velocity drop substantially reduces the contrast between *S*-wave velocities for horizontal or vertical wave propagation with respect to those for $\theta = \pm 45^\circ$ and, thus, diminishes the *S*-wave anisotropy.

5 DISCUSSION AND CONCLUSIONS

The main result of this study is that the connectivity between fractures manifests itself in a pronounced reduction of the velocity anisotropy in the seismic frequency band, which is due to incidence-angle-dependent variations of the stiffening effect of the fracture fluid in response to FPD. This effect, whose expression in the seismic frequency band is particularly prominent in the presence of a low-permeability background, cannot be accounted for using classical elastic approaches. It is important to note that this anisotropy reduction arises when a number of fractures of one set are

intersected by fractures from the other set, but no percolating network is needed. However, the average number of intersections per fracture is an indicator of how close the system is to the percolation threshold. This correlation, together with the fact that velocity anisotropy is a robust attribute commonly employed in the quantitative characterization of fractured rocks, imply that seismic data can be expected to contain information on the effective hydraulic properties.

We consider two sets of orthogonal fractures, which correspond to the most favourable situation for producing FPD effects on seismic velocity anisotropy. For *P*-waves and other intersection angles, both fracture sets will be affected by the propagating wave and, thus, the reduction of fluid stiffening effect for connected fractures will be less significant. For *S*-waves, the induced fluid pressure variations in non-orthogonal fracture sets will not necessarily cancel out when the fractures become connected and, thus, the reduction of anisotropy will also be less prominent. In addition, the analysis presented in this work has been limited to 2-D due to numerical limitations. Even though the infinite extent of the fractures in the third dimension implicitly assumed by our simulations may cause artefacts with regard to the effective properties of rocks with finite-length fractures, the overall nature of the observed connectivity effects are expected to remain valid. The details of how the reduction in anisotropy varies with fracture intersection angle as well as the role of dimensionality of the model will be explored in future works.

In the framework of the linear slip theory (Schoenberg 1980), the role played by fracture connectivity on the stiffening effect of the fluid saturating the fractures could, in principle, be interpreted as corresponding changes in the compliance of the fractures. That is, while the tangential stiffness of fractures is not affected by fluids, the reduced fluid stiffening effect due to the connectivity of fractures tends to increase their normal compliance. In this context, it is interesting to note that there appears to be a link to hydraulic fracture stimulations, as a rise of the ratio of normal to tangential fracture compliance has been observed during such operations (Verdon & Wüstefeld 2013), which may indeed be attributed to an increase of the fracture connectivity. However, further research is needed as the linear slip theory does not account for fracture interaction in general and fracture intersections in particular. In addition, overpressure of the fracture fluid due to hydraulic stimulations and the presence of gas and water in the fractures may alter the FPD process with respect to the scenarios considered in this paper.

The results of this study suggest that temporal variations of seismic anisotropy may be an indicator of changes in fracture connectivity. This observation could have applications in different areas, including the monitoring of stimulated hydrocarbon reservoirs or active volcanic regions, among others. The present contribution may also help to explain potential discrepancies between seismic inversion results pointing to weak velocity anisotropy and other fracture observations, such as borehole televiewer or hydraulic transmissivity data, which from a classical elastic perspective would seem to be concordant with strong anisotropy (e.g. Herwanger *et al.* 2004). For instance, Vécsey *et al.* (1998) observed a decrease of seismic velocity anisotropy in a fractured region of a geothermal reservoir with increasing pressurization. Given that additional fracturing is usually considered to result in an increase of anisotropy, this was rather unexpected at the time. However, in the light of this work, this observation may actually be indicative of an increase of the connectivity degree of the evolving fracture network.

ACKNOWLEDGEMENTS

This work has in part been completed within the Swiss Competence Center for Energy Research - Supply of Electricity, with the support of the Swiss Commission for Technology and Innovation. JGR and TMM acknowledge the financial support of the Fondation Herbette for their visits at the University of Lausanne. The authors thank Doug Angus and an anonymous reviewer for insightful comments.

REFERENCES

Biot, M.A., 1941. General theory of three-dimensional consolidation, *J. Appl. Phys.,* **12,** 155–164.

Caspari, E., Milani, M., Rubino, J.G., Müller, T.M., Quintal, B. & Holliger, K., 2016. Numerical upscaling of frequency-dependent P- and S-wave moduli in fractured porous media, *Geophys. Prospect.,* **64,** 1166–1179.

Grechka, V. & Kachanov, M., 2006. Effective elasticity of rocks with closely spaced and intersecting cracks, *Geophysics,* **71,** D85–D91.

Herwanger, J.V., Worthington, M.H., Lubbe, R., Binley, A. & Khazanehdari, J., 2004. A comparison of cross-hole electrical and seismic data in fractured rock, *Geophys. Prospect.,* **52,** 109–121.

Kachanov, M., 1992. Effective elastic properties of cracked solids: Critical review of some basic concepts, *Appl. Mech. Rev.,* **45,** 304–335.

Liu, E. & Martinez, A., 2012. *Seismic Fracture Characterization: Concepts and Practical Applications,* EAGE.

Liu, E., Hudson, J.A. & Pointer, T., 2000. Equivalent medium representation of fractured rock, *J. geophys. Res.,* **105,** 2981–3000.

Maultzsch, S., Chapman, M., Liu, E. & Li, X.Y., 2003. Modelling frequency-dependent seismic anisotropy in fluid-saturated rock with aligned fractures: Implication of fracture size estimation from anisotropic measurements, *Geophys. Prospect.,* **51,** 381–392.

Rubino, J.G., Guarracino, L., Müller, T.M. & Holliger, K., 2013. Do seismic waves sense fracture connectivity?, *Geophys. Res. Lett.,* **40,** 692–696.

Rubino, J.G., Müller, T.M., Guarracino, L., Milani, M. & Holliger, K., 2014. Seismoacoustic signatures of fracture connectivity, *J. geophys. Res.,* **119,** 2252–2271.

Rubino, J.G., Caspari, E., Müller, T.M., Milani, M., Barbosa, N. & Holliger, K., 2016. Numerical upscaling in 2D heterogeneous poroelastic rocks: anisotropic attenuation and dispersion of seismic waves, *J. geophys. Res.,* **121,** 6698–6721.

Saenger, E.H. & Shapiro, S.A., 2002. Effective velocities in fractured media: a numerical study using the rotated staggered finite-difference grid, *Geophys. Prospect.,* **50,** 183–194.

Schoenberg, M., 1980. Elastic wave behavior across linear slip interfaces, *J. acoust. Soc. Am.,* **68,** 1516–1521.

Tsvankin, I., Gaiser, J., Grechka, V., van der Baan, M. & Thomsen, L., 2010. Seismic anisotropy in exploration and reservoir characterization: an overview, *Geophysics,* **75,** 75A15–75A29.

Vécsey, G., Holliger, K., Pratt, R.G., Dyer, B.C. & Green, A.G., 1998. Anisotropic seismic tomography of a potential hot dry rock reservoir before and during induced pressurization, *Geophys. Res. Lett.,* **25,** 1991–1994.

Verdon, J.P. & Wüstefeld, A., 2013. Measurement of the normal/tangential fracture compliance ratio (Z_N/Z_T) during hydraulic fracture stimulation using S-wave splitting data, *Geophys. Prospect.,* **61,** 461–475.

Will, R., Archer, R. & Dershowitz, B., 2004. A discrete fracture network approach to conditioning petroleum reservoir models using seismic anisotropy and production dynamic data, in *SPE Annual Technical Conference and Exhibition,* 26-29 September, Houston, Texas, Society of Petroleum Engineers, SPE 90487.